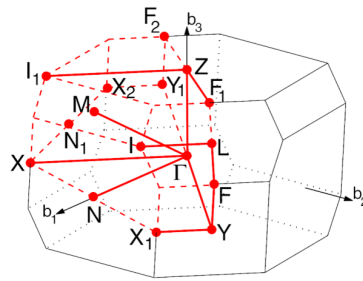


Doping isolated one-dimensional antiferromagnetic semiconductor Vanadium tetrasulfide (VS_4) nanowires with carriers induces half-metallicity

Shuo Li ^a, Junjie He ^{a,b}, Petr Nachtigall ^a, Lukáš Grajciar ^a, Federico Brivio ^a

February 1, 2021

1 Figures



MCLC₁ path: Γ -Y-F-L-||₁-Z- Γ -X|X₁-Y|M- Γ -N|Z-F₁

Figure S1: The high symmetry points of the first Brillouin zone for the band structure of the VS_4 bulk phase. This figure was created from <http://materials.duke.edu/awrapper.html>

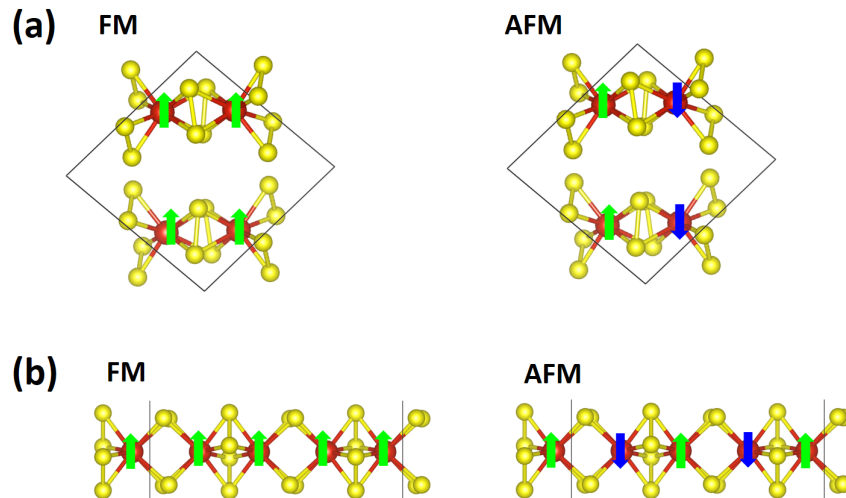


Figure S2: Ferromagnetic (FM) and antiferromagnetic (AFM) states for (a) VS_4 bulk phases and (b) isolated VS_4 nanowires (NWs).

^aDepartment of Physical and Macromolecular Chemistry & Charles University Center of Advanced Materials, Faculty of Science, Charles University, Hlavova 8, 128 43 Prague 2, Czech Republic; E-mail: briviof@natur.cuni.cz

^bBremen Center for Computational Materials Science, University of Bremen, Am Fallturm 1, 28359 Bremen, Germany

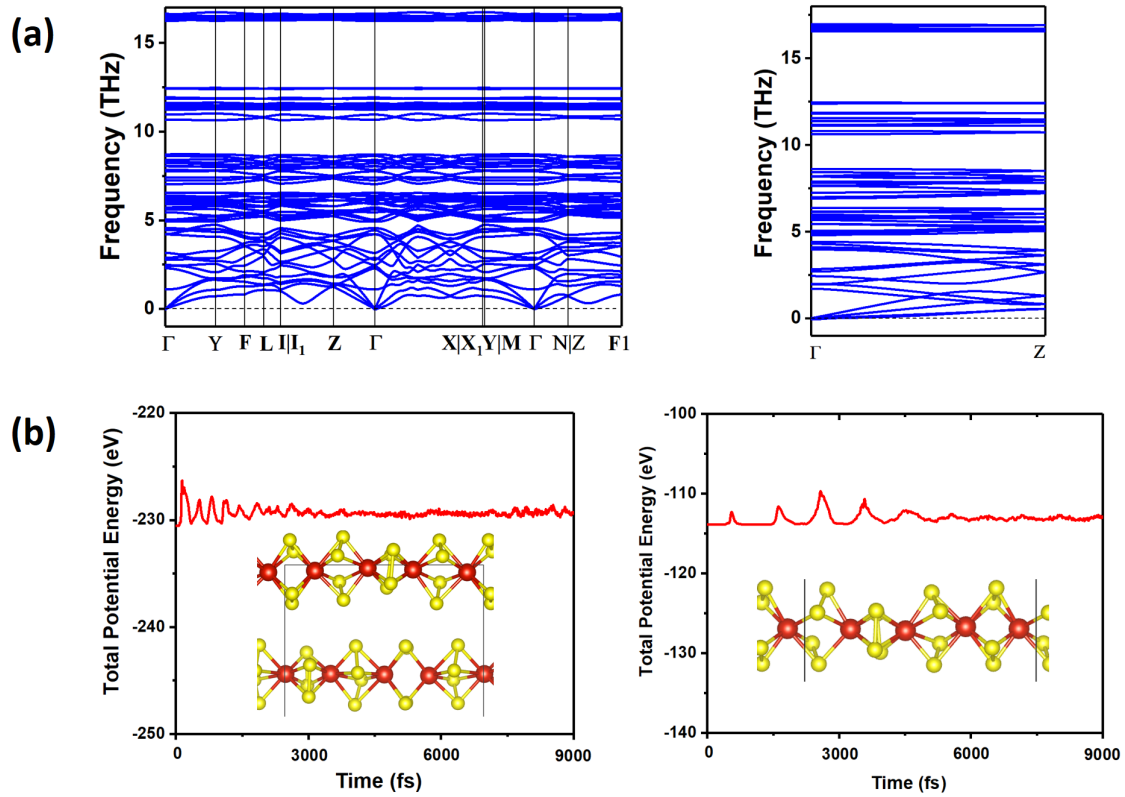


Figure S3: (a) Phonon spectra and (b) total potential energy of NWs as a function of simulation time for the VS₄ bulk phase (conventional cell) and the isolated VS₄ NW by using *ab-initio* molecular dynamics (300K). The inset shows the corresponding structure after the simulation for 9 ps.

T_N is defined as a maximum on the temperature dependent specific heat C_V curve,

$$C_V = (\langle E^2 \rangle - \langle E \rangle^2)/T^2 \quad (1)$$

Where T is the temperature and E is the energy.

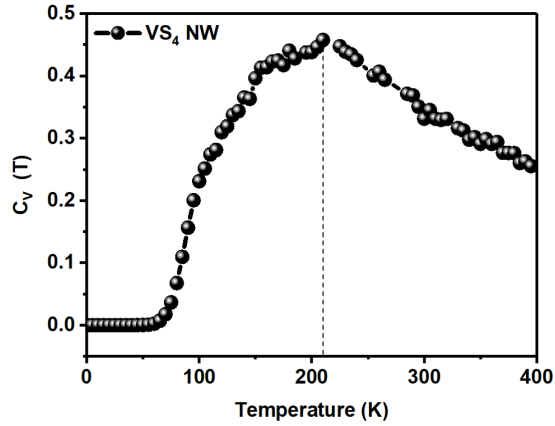


Figure S4: Specific heat calculated for the isolated VS_4 NW with respect to the temperature

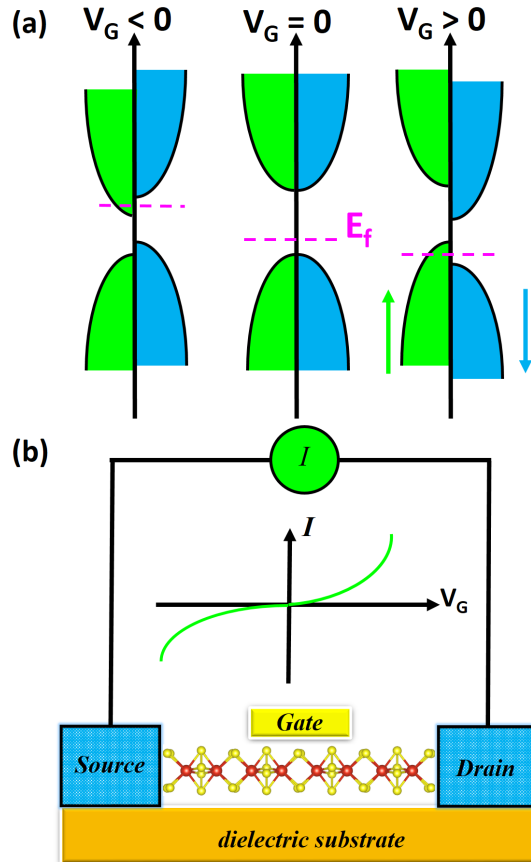


Figure S5: (a) The schematic plot of transformation between the HMAF and AFM states under gate voltages of $V_G < 0$, $V_G = 0$ and $V_G > 0$, respectively. (b) The schematic plot of AFM spintronics device based on the isolated VS_4 NW, together with the $I - V_G$ relationship under the gate voltage. The switching of the spin current can be manipulated by gate voltages.

To evaluate the stability of the isolated VS_4 NW inside BN nanotubes of different sizes, the binding energy (E_b) for the unit cell is calculated as:

$$E_b = E_{total} - E_{NW} - E_{nanotube} \quad (2)$$

where E_{total} stand for the total energies of the isolated VS_4 NW inside the (m, m) BN nanotube. E_{NW} and $E_{nanotube}$ are the energies of the isolated VS_4 NW and the (m, m) BN nanotube. $m = 6, 7, 8$ and 9 , which are the direction of the vector.

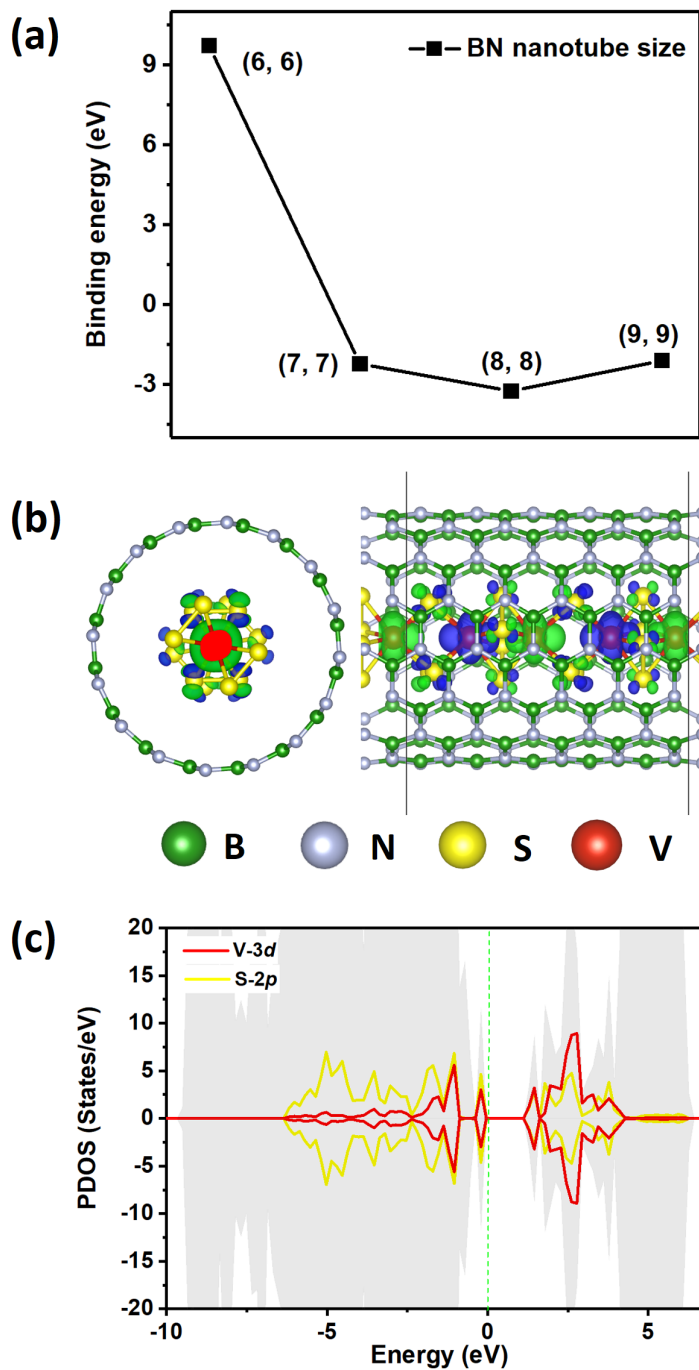


Figure S6: (a) Binding energies E_b of the isolated VS_4 NW inside various BN nanotubes are presented. (b) Spin polarization density of the nanocable. (c) The partial density of states of the nanocable at $PBE + U$ level ($U = 3$). The gray shadow is the total density of states.

Doping isolated one-dimensional antiferromagnetic semiconductor Vanadium tetrasulfide (VS_4) nanowires with carriers induces half-metallicity †

Shuo Li ^a, Junjie He ^{a,b}, Petr Nachtigall ^a, Lukáš Grajciar ^a, Federico Brivio ^a

Quasi one-dimensional (1D) vanadium tetrasulfide (VS_4) nanowires (NWs) are synthetic semiconductors which combine with each other through Van der Waals interactions to form bulk phases. However, the properties of these individual nanowires remain unknown. Nevertheless, our calculations of their stability indicate that VS_4 NWs can be separated from their bulk structures. Accordingly, we theoretically investigated the geometrical, electronic, and magnetic properties of bulk phase and isolated VS_4 NWs. Our results indicate that both bulk phase and isolated VS_4 NWs are semiconductors with band gaps of 2.24 and 2.64 eV, respectively, and that they prefer the antiferromagnetic (AFM) ground state based on DFT calculations. These calculations also suggested that isolated VS_4 NWs show half-metallic antiferromagnetism upon electron and hole doping because carrier doping splits the spin degeneracy to induce local spin polarisation. As a result, spin polarisation currents in isolated VS_4 NWs can be manipulated with locally applied gate voltage. Therefore, these 1D AFM materials have a high potential for advancing both fundamental research and spintronic applications because they are more resistant to magnetic perturbation than their 1D ferromagnetic counterparts.

1 Introduction

Research aimed at improving the performance of electronics has pushed the physical limits of these devices. However, further advances in information technology require developing alternatives to electronics¹⁻⁴. For this purpose, many new methodologies have been proposed, such as molecular electronics, nanoelectronics⁵⁻⁷, spintronics⁸⁻¹⁰, and valleytronics¹¹⁻¹³. Among these new developments, spintronics stands out for its compatibility with conventional electronics. Consequently, spintronics can be used to broaden the possibilities of conventional electronics^{8,14}. In contrast to electronics, in which electrical charges are manipulated to induce a current, spintronics aims to exploit the two spin polarization of unpaired electrons to create a spin-polarised current, thus enhancing the performance of semiconductors, in terms of electrical conductivity and transport of binary information. Accordingly, spintronics enables us to improve the design of logic components, including memory boards and transistors^{15,16}.

Spintronics is based on the ability to control the intrinsic spin of the electron, which was first discovered¹⁷ in ferromagnetic (FM) metals but has since been proved viable in other classes of FM materials, most notably in half-metallic ferromagnets¹⁸. Unlike paramagnetic metals, FM metals have a different density of states for the two spins. Consequently, the latter have a neat magnetic momentum and exhibit a spin-polarised current at adequately low temperatures^{17,19}. Similarly, half-metallic ferromagnets have two spin channels (which guarantees a neat magnetic momentum), but only one of spin channels displays metallic character, whilst the other has a band-gap²⁰. FM materials with non-null magnetic

polarisation have stray fields, which can induce interference between different elements, thus limiting the down-scaling of devices^{10,21-23}). For this reason, most studies have focused on antiferromagnetic (AFM) materials.

AFM materials have been primarily manipulated for spintronics by inducing half-metallic antiferromagnetism (HMAF)²⁴⁻²⁶. HMAF materials were first proposed by H. van Leuken and R. A. de Groot²⁷, who showed that many Heusler compounds, more specifically CrMnSb, could be fully spin-compensated half-metallic materials. Heusler compounds are ternary compounds with two different magnetic centres at different sub-lattices, thus decoupling electronic from magnetic properties. Recently, these theoretical predictions have been experimentally confirmed in similar compounds, namely Half-Heusler: Mn_2RuxGa and Mn_2Pt_xGa alloys^{28,29}. These studies have mostly focused on bulk phases, while low-dimensional materials remain unexplored because their lower dimensionality requires different strategies to remove the spin degeneracy, either applying a bias voltage or using organic-inorganic materials, for example. Gong et al. showed that the bilayer $2H-VSe_2$ becomes HMAF when applying proper electric fields³⁰, while Ai *et al.* designed a two-dimensional (2D) metal-organic HMAF ($CoFePz$), which paved the way to the development of organic HMAF³¹. Among its potential applications of HMAF, spin field-effect transistors (FET)^{30,32} stand out for their ability to control the spin current³³. Moreover, carrier doping enables us to manipulate the electronic and magnetic properties of low-dimensional materials, which are theoretically and experimentally accessible³⁴⁻³⁶. Therefore, carrier doping is an effective strategy to control the spin current in low-dimensional magnetic materials. Few materials, for example $NbSe_3$ ³⁷, can be isolated as true one-dimensional (1D) materials, which are joined in quasi-1D materials through Van der Waals forces. Some 1D compounds have been proposed as candidates for spintronic applications, including metal trihydride molecular nanowires³⁸ (NWs), 1D metal benzenetetramine coordination polymers³⁹, Co-dithiolenene molecular wires⁴⁰, transition metal tribromide NWs⁴¹, transition metal trichalcogenide NWs^{37,42}, and transition metal chalcogenide NWs⁴³. These materials have been theoretically investigated for their electronic and magnetic properties, but not as much for their spintronic properties, due to the lack of experimental reports.

The Vanadium tetrasulfide (VS_4) is found in nature as a mineral, and was discovered in 1906⁴⁴. Its linear chain-like structure is composed of two S_2^{2-} moieties connecting V^{4+} centers. The different chains are bound together by Van der Waals forces to form nano-rods in quasi-1D compounds⁴⁵⁻⁴⁷. VS_4 NWs have been studied for other applications, such as batteries, capacitors, and photocatalysts^{45,48-51}. The possible oxidation states of Vanadium ions induce different magnetic properties that have been demonstrated in different materials: Vanadium dichalcogenides (VX_2 , $X = S, Se$) monolayers, MXenes (VX_2 , $X = C, N$)^{52,53}, and Haeckelite VS_2 ⁵⁴. However, the geometric, electronic and magnetic properties of VS_4 as a 1D NW are not clearly understood yet. This study aimed to assess how the magnetic properties of VS_4 are affected by its dimensionality and how VS_4 can be used for spintronic applications.

2 Methods

All calculations were performed within the density functional theory (DFT) as implemented in the Vienna *ab-initio* simulation package (VASP)^{55,56}. The structural properties have been determined using the Perdew Burke Ernzerhof (PBE) version of the generalised gradient approximation (GGA)⁵⁷, while the electronic and mag-

^aDepartment of Physical and Macromolecular Chemistry & Charles University Center of Advanced Materials, Faculty of Science, Charles University in Prague, Hlavova 8, 128 43 Prague 2, Czech Republic; E-mail: briviof@natur.cuni.cz

^bBremen Center for Computational Materials Science, University of Bremen, Am Fallturm 1, 28359 Bremen, Germany

netic properties have been calculated with the hybrid HSE06⁵⁸ functional. The dispersion forces have been included in the DFT-D3 method⁵⁹. An energy cut-off of 500 eV was employed to define the plane-wave basis sets, considering the wavefunction converged for total energy variations below 10^{-6} eV. The same parameters have been used for both PBE and HSE06 calculations. The structures were fully optimised to minimise the forces below -0.02 eV/Å. For both geometry relaxation and electronic properties in the Brillouin zone, this material was sampled using a Monkhorst–Pack k-point mesh of $5 \times 5 \times 5$ and $1 \times 1 \times 5$ for the bulk phase and isolated NWs, respectively. The isolated NW was simulated including a vacuum space of 15 Å in the x and y directions. The high symmetry points of the first Brillouin zone for the band structure of the VS₄ bulk phase are shown in Figure S1. We calculated phonon spectra using the finite differences method, as implemented in VASP. Post-processing and analysis have been performed using the software PhonoPy⁶⁰. For this task, we have used tighter convergence criteria, more specifically 10^{-8} eV for the wavefunction and -0.001 eV/Å for the forces. In addition, we address the kinetic stability of the structures performing a set of *ab-initio* molecular dynamics (AIMD) calculations, as implemented in VASP. These calculations have been completed using the Nosé algorithm⁶¹ in the NVT ensemble at room temperature (300 K) for the duration of 9 ps. The formation energy (E_{form}) of each VS₄ unit formula is calculated as:

$$E_{\text{form}} = E(\text{VS}_4)/n - E(\text{V}) - 4E(\text{S}) \quad (1)$$

where $E(\text{VS}_4)$ is the total energy of the VS₄ bulk phase or the isolated NW containing n unit formula, while $E[\text{V}]$ and $E[\text{S}]$ are the single atom energies from the bulk phases of cubic V and S⁶². Carrier doping was simulated by removing or adding electrons from the system with the homogeneous background charge to keep charge neutrality.

The magnetic properties have been analysed using a collinear model for simplicity. We considered FM and AFM states to calculate the preferred magnetic ground state structures of NW (Figure S2). To account for these effects, we used the Monte Carlo method to solve a simple Ising model⁶³:

$$H = -\sum_{ij} J_{\text{intra}} M_i \cdot M_j \quad (2)$$

where J_{intra} is the nearest-neighbour exchange-coupling parameter of intra-NWs and M is the spin magnetic moment per chemical formula. The J_{intra} value can be calculated by the exchange energy ($E_{\text{ex}} = E_{\text{FM}} - E_{\text{AFM}}$). The exchange coupling parameters have been used to calculate the Néel temperature (T_{N}) performing a Monte Carlo simulation on a 150 1D chain lattice with 10^{-5} steps for each temperature using the open-source software ALPS⁶⁴.

3 Results

3.1 Structural analysis

Figure 1a shows the primitive cell of VS₄ bulk phase (C2/c #15) in which each V atom is coordinated with eight S atoms forming four dimers. From the bulk phase, we have built the isolated NW unit cell (Figure 1b). The geometric data on the VS₄ bulk phase and on the isolated VS₄ NW are summarised in Table 1. Both the bulk and isolate NW phases of VS₄ are dynamically stable, as shown by the absence of an imaginary frequency in the phonon dispersion (figure S3a). The stability of these materials is also confirmed by AIMD simulation at room temperature, thus suggesting that individual NWs can be isolated (figure S3b).

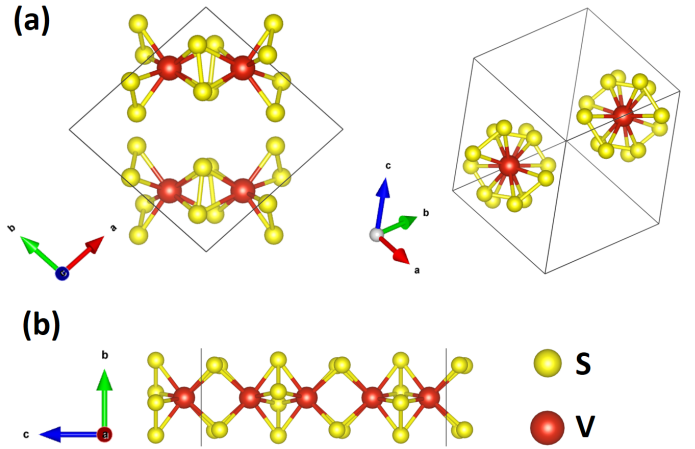


Figure 1 (a) Primitive cell of the VS₄ bulk phase from two directions, that is, along (001) direction, on the left panel, and along (111) direction, on the right panel. (b) Isolated VS₄ NW. The repeating units are marked by the black lines.

3.2 Electronic and magnetic properties

We now focus on the electronic and magnetic properties of the VS₄ bulk phase and the isolated NW. Both the bulk phase and the isolated NW have an AFM ground state, and their stability is given by E_{ex} , as outlined in Table 1. The magnetic momentum of V is similar in the bulk phase and in the isolated NW, with values of 1.15 and 1.17 μ_{B} , respectively. The bulk phase has an indirect band gap of 2.24 eV between the Y and Z points of the Brillouin Zone. The calculated electronic band gap largely overestimated the experimental optical band gap of VS₄ films (approximately 1.35 eV)⁴⁵ which is usually observed in similar cases^{65–67}. This difference of band gaps could be attributed to the experimental conditions in which the optoelectronic properties depend on the sulfur partial pressure of synthesis and on the morphology of the sample⁴⁵. Most importantly, our model for the bulk phase assumes perfect crystallinity, which is unlikely to occur in the family of low-dimensional compounds.

The spin density (Figure 2b) shows the AFM G-type motif of the material⁶⁸. The valence band maximum (VBM) and the conduction band minimum (CBM) of the VS₄ bulk phase are formed by the overlap of S 2*p* orbitals with V 3*d* levels as shown in the partial density of states (PDOS) (Figure 2a). The V 3*d* orbitals split into a non-degenerate d_{z^2} orbital and into two 2-fold degenerate d_{xz}/d_{yz} and $d_{xy}/d_{x^2-y^2}$ orbitals. The local V 3*d* orbitals can induce an antiparallel spin arrangement on neighboring V via the double-exchange mechanism (Figure 2b). The VBM and CBM of the VS₄ bulk phase derive from the S 2*p* orbitals and V $d_{xz} + d_{yz}$ orbitals (Figure 2c), in line with its PDOS.

The electronic structure of the isolated VS₄ NW reflects the lower dimensionality of the material, which induces a larger band-gap of 2.65 eV with a higher density of state (Figure 3a). The lack of interactions between different chains of VS₄ affects the nature of the bond. We can observe a larger contribution of VBM and CBM in the isolated VS₄ NW due to the S 2*p* states (Figure 3a). The VBM and the CBM of the V 3*d* orbitals of the isolated NW are different from those of the bulk phase. V $d_{xy}/d_{x^2-y^2}$ orbitals of the isolated VS₄ NW contribute to the VBM and CBM.

To further understand the change of electronic and magnetic properties between the VS₄ bulk phase and the isolated VS₄ NW, we plotted the electron localisation function (ELF) for the VS₄ bulk

Table 1 Structural parameters, electronic and magnetic properties of the bulk phase and isolated NW for VS_4 . E_{form} is the formation energy (eV). $L_{\text{S-dimer}}$ is S dimer bond-length (Å). $L_{\text{V-V}}$ is the V-V bond length. $L_{\text{V-S}}$ is the V-S bond length. E_{g} is the band gap. E_{ex} is the exchange energy (eV). μ_{B} is the local magnetic moment of the V atoms.

configurations	E_{form}	$L_{\text{S-dimer}}$	$L_{\text{V-V}}$	$L_{\text{V-S}}$	E_{g}	E_{ex}	μ_{B}
Bulk	-2.59	2.03	2.77, 3.20	2.54, 2.39	2.24	0.961	1.15
NW	-2.06	2.03	2.77, 3.22	2.55, 2.39	2.65	0.948	1.17

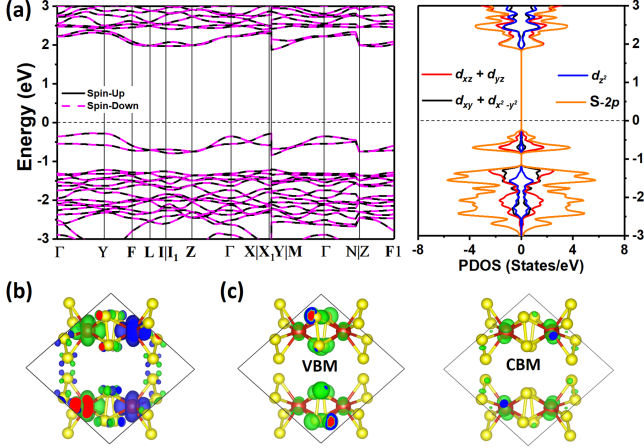


Figure 2 (a) Band structures and PDOS and (b) spin-polarised density of the VS_4 bulk phase, where spin-up and spin-down densities are shown in green and blue, respectively. (c) The valence band maximum (VBM) and the conduction band minimum (CBM) are shown in green. The isosurface is $0.005 e \cdot \text{Bohr}^{-3}$.

phase and for the isolated VS_4 NW (Figure 4). The ELF of S atoms in the VS_4 bulk phase is more localised than that of the isolated VS_4 NW due to Van der Waals interactions of NWs in the VS_4 bulk phase. Moreover, VS_4 NW has distinct characteristics of localised d electrons of V atoms: more relatively itinerant V d electrons in the isolated VS_4 NW than that in the VS_4 bulk phase. Itinerant d electrons of V atoms can induce spin polarisation of neighbouring S atoms, *e.g.*, an anti-parallel spin arrangement via a double-exchange mechanism. While the PDOS of d orbitals of V atoms differ between the VS_4 bulk phase and the isolated VS_4 NW. This difference in electronic properties does not affect the AFM character of these materials with a double-exchange mechanism, which also depends on the V atoms.

3.3 Macroscopic magnetic properties

Magnetic order is more susceptible to temperature in materials with lower dimensionality⁶⁹ due to the lower number of interactions. As a result, magnetic fluctuation, which destroys the order, is more likely to happen in low-dimensional materials than in three-dimensional materials. DFT calculations enable us to directly determine the magnitude of such interactions, but the value of T_{N} cannot be simulated since it emerges as a statistic average. Nevertheless, we employed exchange interactions (obtained *ab-initio*) to describe the Temperature dependence of our system using an Ising model solved with a Monte Carlo approach. For the isolated VS_4 NW, we obtained a T_{N} of 210 K (Figure S4).

3.4 HMAF based FET

Previous studies have shown that carrier doping manipulates spin currents through the voltage gate^{34,36}. We analysed doping concentrations of 0.1, 0.3, and 0.5 electron (and hole) per unit

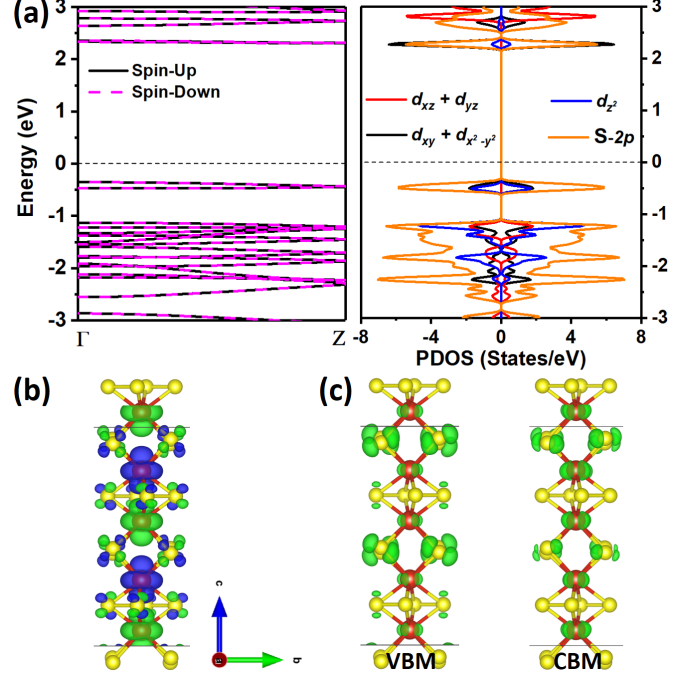


Figure 3 (a) Band structures and PDOS and (b) spin polarised density of the isolated VS_4 NW, where spin-up and spin-down densities are shown in green and blue, respectively. (c) VBM and CBM are shown in green. The isosurface is $0.005 e \cdot \text{Bohr}^{-3}$.

cell of the isolated VS_4 NW (equivalent to $0.83, 2.50, \text{ and } 4.17 \times 10^6 \text{ cm}^{-1}$). The isolated VS_4 NW with carrier doping is HMAF, exhibiting complete spin-polarisation around the Fermi level (Figure 5). Because carrier doping shifts the Fermi level and spin polarisation of S and V atoms, PDOS for the isolated VS_4 NW with carrier doping show metallic states in the spin-up channel and semiconductor states (band gaps are over $2 eV$.) in the spin-down channel. These effects are detected as small perturbations of the small AFM, which can be considered preserved for practical applications. The main contributions to the metallic states around the Fermi level derive from V $d_{xy}/d_{x^2-y^2}$ orbitals and S $2p$ orbitals.

The magnetic momentum of V atoms is affected by carrier doping, and the magnetic momentum of each S atom is very small. When doping with 0.5 electron, the magnetic momentum of one V atom (marked 4) increases from 1.17 to $1.46 \mu_{\text{B}}$ (Figure 6a). When doping with 0.5 hole, the magnetic momentum of one V atom decreases from 1.17 to $1.08 \mu_{\text{B}}$ (Figure 6a). The isolated VS_4 NW retains its AFM state. The E_{ex} is rapidly decreased under hole doping and increased under electron doping. Our results indicate that the AFM state of the isolated VS_4 NW is stable when injected with a low concentration of carriers. Moreover, we visualise the partial charge density (around Fermi level) of the isolated VS_4 NW at 0.5 electron and hole doping (Figure 6c). The participation of V and S orbitals also differs: formed by V $d_{xy}/d_{x^2-y^2}$ and

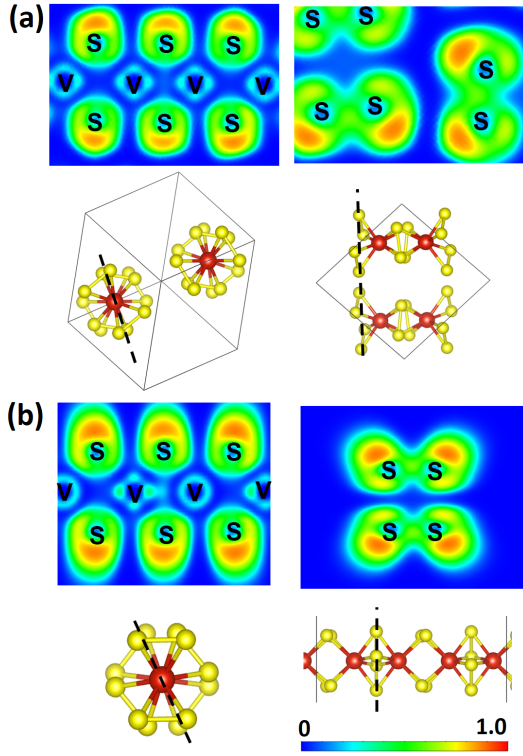


Figure 4 Electron localisation function (ELF) maps of (a) the VS_4 bulk phase and (b) isolated VS_4 NW. The dot line is the chosen direction of the ELF slice. The unit of the color scale is "probability".

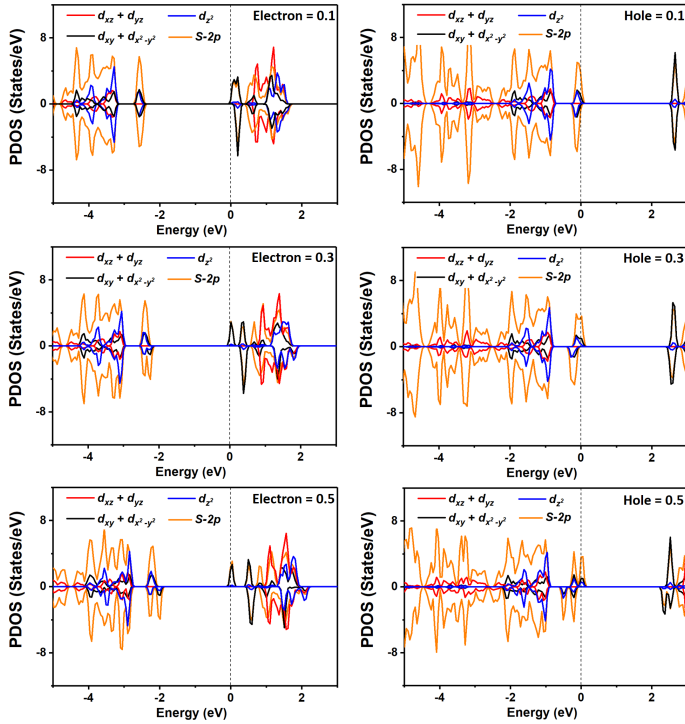


Figure 5 PDOS of the isolated VS_4 NW under carrier doping with a carrier concentration of 0.1, 0.3 and 0.5 electron (and hole) per unit cell.

$S\ 2p$ orbitals at 0.5 electron doping and by $V\ d_{xy}/d_{x^2-y^2}$, d_{z^2} and more $S\ 2p$ orbitals at 0.5 hole doping.

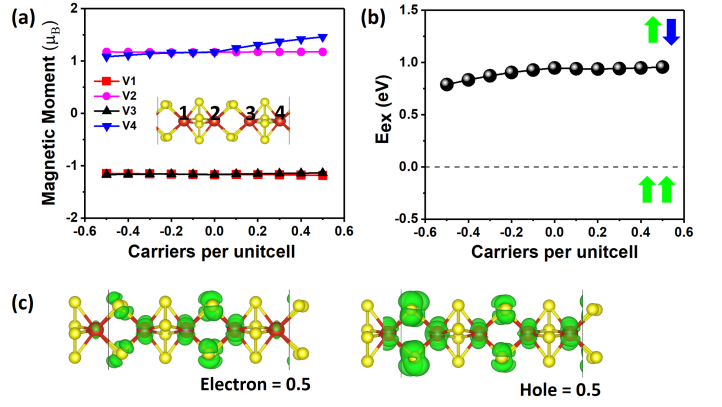


Figure 6 (a) Local magnetic moment on each V atom of the isolated VS_4 NW with carrier doping. (b) Exchange energy (E_{ex}) under different carrier concentrations of the isolated VS_4 NW. The positive and negative values refer to electron and hole doping, respectively. The up and down arrows indicate up- and down-spin, respectively. (c) partial charge density (around the Fermi level) of the isolated VS_4 NW with 0.5 electron and hole doping.

4 Discussion

Our results indicate that the isolated VS_4 NW is an AFM semiconductor with a high T_N of 210 K. This is an important result because ferromagnetic 1D materials, such as the quasi-1D organic ferromagnet ($T_C\ 0.56\ K$)⁷⁰, the tribromide NW of the half-metal VBr_3 ($T_C\ 80\ K$)⁴¹, the trihydride molecular NW of the half-metal CoH_3 ($T_C\ 98\ K$)³⁸ and transition metal dihalide nanowires $CuCl_2$ ($T_C\ 14\ K$)⁷¹, usually have much lower Curie temperatures (T_C). Furthermore, T_N of the isolated VS_4 NW is well above the temperature of liquid nitrogen (77K) and is also higher than that of different 2D antiferromagnets, such as bilayer CrI_3 ($T_N\ 45K$)⁷² or polyradical nanosheets (42.5K)⁷³. An even better prediction T_N could be obtained for the isolated VS_4 NW, but this prediction is a promising starting point for further experimental characterisation.

Moreover, the AFM character and large band gap of the isolated NWs prevent spin-polarised currents in VS_4 . The local spin polarisation of ideal antiferromagnetism, which in turn allows spin-polarised currents, could be a technological solution³⁶. Here, we consider a model where carriers are injected into our materials, a process commonly known as carrier doping in the literature, in analogy to chemical doping⁷⁴. A method for carrier doping consists of building a spin FET device (scheme shown in Figure S5) where the charges are injected by applying different gate voltages.

The influence of the environment on the transport properties and electrical contacts of NWs limit their applications. Therefore, protecting NWs by preserving the electronic and magnetic properties of the isolated VS_4 NW should be tested in spintronic applications. Nanotubes may protect NWs by preventing oxidation and maintaining electronic and magnetic properties unchanged^{37,41}, and nanocables, composed of insulating outer sheaths and a NW core, may guide the design of the models. Here, a designed nanocable on the isolated VS_4 NW and a $1 \times 1 \times 5$ (8, 8) boron nitride (BN) zigzag nanotube is constructed (Figure S6), where the lattice mismatch is approximately 4.5%. The isolated VS_4 NW has a slight strain. The distance between the NW and the wall of the BN nanotube is approximately 3.57 Å. The electronic and magnetic properties of the VS_4 -BN nanocable is similar to that of the isolated VS_4 NW. Therefore, the spin polarisation of the nanocable mainly derives from the inner NW, while the outer nanotube has

a negligible effect on the nanocable. Such a hybrid structure may also enable interesting applications in spintronics.

5 Summary

We presented herein a new strategy in VS_4 NWs towards AFM spintronics. The VS_4 NWs are bound together by Van der Waals forces to form nano-rods in quasi-1D compounds in experiments. In this context, the geometric, electronic and magnetic properties of the VS_4 bulk phase and isolated VS_4 NW were analysed. First, we investigated the stability of the VS_4 bulk phase and isolate VS_4 NW by formation energy, AIMD and phonon spectra. After confirming the stability of VS_4 NWs, we investigated the electronic and magnetic properties of VS_4 NWs. The magnetic ground states of the isolate VS_4 NW is AFM with a high Néel temperature (210 K). Detecting and manipulating the spin of AFM materials remains a major challenge due to spin degeneracy in the band structure. Nevertheless, carrier doping can separate the spin degeneracy to induce local spin polarisation. The isolated VS_4 NW represent the half-metallic antiferromagnet resulting from carrier doping, which can be achieved with gate voltages. Our results indicate that the isolated VS_4 NW is a promising 1D material for AFM spintronic applications. Carrier doping induces a rigid shift in the Fermi level into the valence or conduction bands, resulting in a complete spin-polarisation of carriers, which can be induced by applying a gate voltage. Thus, spin polarisation currents can be manipulated by applying a gate voltage, with a high potential for spintronic applications. We further considered the protection of NWs. BN nanotubes can provide protection by preventing oxidation and by preserving the electronic and magnetic properties of VS_4 NWs. Our results open up new opportunities for applying 1D NWs in AFM spintronics by inducing half-metallic antiferromagnetism.

6 Conflicts of interest

There are no conflicts to declare.

7 Acknowledgements

Charles University Centre of Advanced Materials (CUCAM) (OP VVV Excellent Research Teams, Project No. CZ.02.1.01/0.0/0.0/15_003/0000417) is acknowledged. S. L. acknowledges the support from GAUK project (Grant No. 792218). The results from this research have been achieved using the DECI resource Kay based in Poblacht na hÉireann at ICHEC with support from the PRACE DECI-16 16DECI0034 CABLE project. We also acknowledge the computer resources, technical expertise, and assistance provided by IT4Innovations National Supercomputing Center. We thank Carlos V. Melo Carlos for editing the manuscript.

Notes and references

- [1] J. A. Del Alamo, *Nature*, 2011, **479**, 317.
- [2] K. Tomioka, M. Yoshimura and T. Fukui, *Nature*, 2012, **488**, 189.
- [3] I. Ferain, C. A. Colinge and J.-P. Colinge, *Nature*, 2011, **479**, 310.
- [4] C. A. Mack, *IEEE Transactions on Semiconductor Manufacturing*, 2011, **24**, 202–207.
- [5] W. Lu and C. M. Lieber, *Nanoscience And Technology: A Collection of Reviews from Nature Journals*, World Scientific, 2010, pp. 137–146.
- [6] D. Akinwande, N. Petrone and J. Hone, *Nature Communications*, 2014, **5**, 5678.
- [7] C. Berger, Z. Song, T. Li, X. Li, A. Y. Ogbazghi, R. Feng, Z. Dai, A. N. Marchenkov, E. H. Conrad, P. N. First *et al.*, *The Journal of Physical Chemistry B*, 2004, **108**, 19912–19916.
- [8] S. Wolf, D. Awschalom, R. Buhrman, J. Daughton, S. Von Molnar, M. Roukes, A. Y. Chtchelkanova and D. Treger, *science*, 2001, **294**, 1488–1495.
- [9] C. Felser, G. H. Fecher and B. Balke, *Angewandte Chemie International Edition*, 2007, **46**, 668–699.
- [10] X. Li and J. Yang, *National Science Review*, 2016, **3**, 365–381.
- [11] J. R. Schaibley, H. Yu, G. Clark, P. Rivera, J. S. Ross, K. L. Seyler, W. Yao and X. Xu, *Nature Reviews Materials*, 2016, **1**, 16055.
- [12] D. Zhong, *Science Advances*, 2017, **3**, e1603113.
- [13] T. Jungwirth, J. Sinova, A. Manchon, X. Marti, J. Wunderlich and C. Felser, *Nature Physics*, 2018, **14**, 200–203.
- [14] I. Žutić, J. Fabian and S. D. Sarma, *Reviews of Modern Physics*, 2004, **76**, 323.
- [15] A. V. Chumak, V. I. Vasyuchka, A. A. Serga and B. Hillebrands, *Nature Physics*, 2015, **11**, 453–461.
- [16] K. Y. Camsari, S. Ganguly and S. Datta, *Scientific reports*, 2015, **5**, 10571.
- [17] N. F. Mott, *Proceedings of the Royal Society of London. Series A-Mathematical and Physical Sciences*, 1936, **156**, 368–382.
- [18] S. Picozzi, *Frontiers in Physics*, 2014, **2**, 10.
- [19] N. F. Mott, *Proceedings of the Royal Society of London. Series A-Mathematical and Physical Sciences*, 1936, **153**, 699–717.
- [20] X. Li and J. Yang, *Wiley Interdisciplinary Reviews: Computational Molecular Science*, 2017, **7**, e1314.
- [21] T. Jungwirth, X. Marti, P. Wadley and J. Wunderlich, *Nature Nanotechnology*, 2016, **11**, 231.
- [22] V. Baltz, A. Manchon, M. Tsoi, T. Moriyama, T. Ono and Y. Tserkovnyak, *Reviews of Modern Physics*, 2018, **90**, 015005.
- [23] A. H. MacDonald and M. Tsoi, *Philosophical Transactions of the Royal Society A: Mathematical, Physical and Engineering Sciences*, 2011, **369**, 3098–3114.
- [24] X. Hu, *Advanced Materials*, 2012, **24**, 294–298.
- [25] J. He, P. Zhou, N. Jiao, X. Chen, W. Lu and L. Sun, *RSC Advances*, 2015, **5**, 46640–46647.
- [26] Y.-m. Nie and X. Hu, *Physical Review Letters*, 2008, **100**, 117203.
- [27] H. Van Leuken and R. De Groot, *Physical Review Letters*, 1995, **74**, 1171.
- [28] A. K. Nayak, M. Nicklas, S. Chadov, P. Khuntia, C. Shekhar, A. Kalache, M. Baenitz, Y. Skourski, V. K. Guduru, A. Puri *et al.*, *Nature Materials*, 2015, **14**, 679.

- [29] H. Kurt, K. Rode, P. Stamenov, M. Venkatesan, Y.-C. Lau, E. Fonda and J. Coey, *Physical Review Letters*, 2014, **112**, 027201.
- [30] S.-J. Gong, C. Gong, Y.-Y. Sun, W.-Y. Tong, C.-G. Duan, J.-H. Chu and X. Zhang, *Proceedings of the National Academy of Sciences*, 2018, **115**, 8511–8516.
- [31] H. Ai, X. Liu, B. Yang, X. Zhang and M. Zhao, *The Journal of Physical Chemistry C*, 2018, **122**, 1846–1851.
- [32] P. Chuang, S.-C. Ho, L. W. Smith, F. Sfigakis, M. Pepper, C.-H. Chen, J.-C. Fan, J. Griffiths, I. Farrer, H. E. Beere *et al.*, *Nature Nanotechnology*, 2015, **10**, 35–39.
- [33] Y. Deng, Y. Yu, Y. Song, J. Zhang, N. Z. Wang, Z. Sun, Y. Yi, Y. Z. Wu, S. Wu, J. Zhu *et al.*, *Nature*, 2018, **563**, 94–99.
- [34] X. Li, X. Wu and J. Yang, *Journal of the American Chemical Society*, 2014, **136**, 11065–11069.
- [35] H. Yuan, H. Shimotani, A. Tsukazaki, A. Ohtomo, M. Kawasaki and Y. Iwasa, *Advanced Functional Materials*, 2009, **19**, 1046–1053.
- [36] J. He, G. Ding, C. Zhong, S. Li, D. Li and G. Zhang, *Nanoscale*, 2019, **11**, 356–364.
- [37] T. Pham, S. Oh, P. Stetz, S. Onishi, C. Kisielowski, M. L. Cohen and A. Zettl, *Science*, 2018, **361**, 263–266.
- [38] X. Li, H. Lv, J. Dai, L. Ma, X. C. Zeng, X. Wu and J. Yang, *Journal of the American Chemical Society*, 2017, **139**, 6290–6293.
- [39] Y. Wan, Y. Sun, X. Wu and J. Yang, *The Journal of Physical Chemistry C*, 2018, **122**, 989–994.
- [40] T. Zhang, L. Zhu and G. Chen, *Journal of Materials Chemistry C*, 2016, **4**, 10209–10214.
- [41] S.-s. Li, Y.-p. Wang, S.-j. Hu, D. Chen, C.-w. Zhang and S.-s. Yan, *Nanoscale*, 2018, **10**, 15545–15552.
- [42] H. Ye, L. Wang, S. Deng, X. Zeng, K. Nie, P. N. Duchesne, B. Wang, S. Liu, J. Zhou, F. Zhao *et al.*, *Advanced Energy Materials*, 2017, **7**, 1601602.
- [43] C. Shang, L. Fu, S. Zhou and J. Zhao, *JACS Au*, 2020, <https://doi.org/10.1021/jacsau.0c00049>.
- [44] W. Hillebrand, *Journal of the American Chemical Society*, 1907, **29**, 1019–1029.
- [45] E. Flores, E. Munoz-Cortes, J. Bodega, O. Caballero-Calero, M. Martin-Gonzalez, C. Sanchez, J. R. Ares and I. J. Ferrer, *ACS Applied Energy Materials*, 2018, **1**, 2333–2340.
- [46] Y. Zhou, Y. Li, J. Yang, J. Tian, H. Xu, J. Yang and W. Fan, *ACS Applied Materials & Interfaces*, 2016, **8**, 18797–18805.
- [47] G. Lui, G. Jiang, A. Duan, J. Broughton, J. Zhang, M. W. Fowler and A. Yu, *Industrial & Engineering Chemistry Research*, 2015, **54**, 2682–2689.
- [48] C. S. Rout, B.-H. Kim, X. Xu, J. Yang, H. Y. Jeong, D. Odhkuu, N. Park, J. Cho and H. S. Shin, *Journal of the American Chemical Society*, 2013, **135**, 8720–8725.
- [49] R. Sun, Q. Wei, Q. Li, W. Luo, Q. An, J. Sheng, D. Wang, W. Chen and L. Mai, *ACS Applied Materials & Interfaces*, 2015, **7**, 20902–20908.
- [50] S. Wang, F. Gong, S. Yang, J. Liao, M. Wu, Z. Xu, C. Chen, X. Yang, F. Zhao, B. Wang *et al.*, *Advanced Functional Materials*, 2018, **28**, 1801806.
- [51] Y. Wang, Z. Liu, C. Wang, X. Yi, R. Chen, L. Ma, Y. Hu, G. Zhu, T. Chen, Z. Tie *et al.*, *Advanced Materials*, 2018, **30**, 1802563.
- [52] G. Gao, G. Ding, J. Li, K. Yao, M. Wu and M. Qian, *Nanoscale*, 2016, **8**, 8986–8994.
- [53] N. C. Frey, A. Bandyopadhyay, H. Kumar, B. Anasori, Y. Gogotsi and V. B. Shenoy, *ACS nano*, 2019, **13**, 2831–2839.
- [54] Y. Ma, A. Kuc, Y. Jing, P. Philipsen and T. Heine, *Angewandte Chemie International Edition*, 2017, **56**, 10214–10218.
- [55] G. Kresse, *Physical Review B*, 1993, **47**, 558.
- [56] G. Kresse, *Physical Review B*, 1999, **59**, 1758.
- [57] J. P. Perdew, K. Burke and M. Ernzerhof, *Physical Review Letters*, 1996, **77**, 3865.
- [58] J. Heyd, G. E. Scuseria and M. Ernzerhof, *The Journal of Chemical Physics*, 2003, **118**, 8207–8215.
- [59] S. Grimme, J. Antony, S. Ehrlich and H. Krieg, *The Journal of Chemical Physics*, 2010, **132**, 154104.
- [60] A. Togo and I. Tanaka, *Scr. Mater.*, 2015, **108**, 1–5.
- [61] S. Nosé, *The Journal of Chemical Physics*, 1984, **81**, 511–519.
- [62] Y. Watanabe, *Acta Crystallographica Section B: Structural Crystallography and Crystal Chemistry*, 1974, **30**, 1396–1401.
- [63] B. M. McCoy and T. T. Wu, *The two-dimensional Ising model*, Courier Corporation, 2014.
- [64] A. F. Albuquerque, F. Alet, P. Corboz, P. Dayal, A. Feiguin, S. Fuchs, L. Gamper, E. Gull, S. Gürtler, A. Honecker *et al.*, *Journal of Magnetism and Magnetic Materials*, 2007, **310**, 1187–1193.
- [65] T. Zhou, Z. Zang, J. Wei, J. Zheng, J. Hao, F. Ling, X. Tang, L. Fang and M. Zhou, *Nano Energy*, 2018, **50**, 118 – 125.
- [66] S. Ur Rehman, Z. Li, H. Li and Z. Ding, *Physica B: Condensed Matter*, 2017, **524**, 163 – 172.
- [67] P. Lou and J. Y. Lee, *The Journal of Chemical Physics*, 2019, **150**, 184307.
- [68] T. Hotta, S. Yunoki, M. Mayr and E. Dagotto, *Physical Review B*, 1999, **60**, 15009–15012.
- [69] P. Gambardella, *Magnetic Nanostructures in Modern Technology*, Dordrecht, 2008, pp. 325–342.
- [70] M. Takahashi, P. Turek, Y. Nakazawa, M. Tamura, K. Nozawa, D. Shiomi, M. Ishikawa and M. Kinoshita, *Physical Review Letters*, 1991, **67**, 746.
- [71] X. Tan, L. Liu, H. Xiang, G.-F. Du, A. Lou and H.-H. Fu, *Nanoscale*, 2020, **12**, 8942–8948.

- [72] B. Huang, G. Clark, D. R. Klein, D. MacNeill, E. Navarro-Moratalla, K. L. Seyler, N. Wilson, M. A. McGuire, D. H. Cobden, D. Xiao *et al.*, *Nature Nanotechnology*, 2018, **13**, 544–548.
- [73] Y. Yang, C. Liu, X. Xu, Z. Meng, W. Tong, Z. Ma, C. Zhou, Y. Sun and Z. Sheng, *Polymer Chemistry*, 2018, **9**, 5499–5503.
- [74] K. Ueno, S. Nakamura, H. Shimotani, H. Yuan, N. Kimura, T. Nojima, H. Aoki, Y. Iwasa and M. Kawasaki, *Nature Nanotechnology*, 2011, **6**, 408.